Journal of Zhejiang University-SCIENCE A (Applied Physics & Engineering) 2024 25(3):268-274
www.jzus.zju.edu.cn; www.springer.com/journal/11582
E-mail: jzus_a@zju.edu.cn

Research Article

https://doi.org/10.1631/jzus.A2300250

Synthesis and characterization of three new solid polyoxometalates based on Wells-Dawson-derived sandwich-type polyanions $[Co_4(H_2O)_2(P_2W_{15}O_{56})_2]^{16-}$

Jijie YE, Xuan XU, Chuande WU✉

Department of Chemistry, Zhejiang University, Hangzhou 310058, China

Abstract: Three polyoxometalate-based hybrid coordination materials, $[Co_8(H_2O)_{34}(pz)_2\{Co_4(H_2O)_2P_4W_{30}O_{112}\}]\cdot 16H_2O$ (compound 1), $[H_3O]_4[Co_6(H_2O)_{22}(pz)_2\{Co_4(H_2O)_2P_4W_{30}O_{112}\}]\cdot 21H_2O$ (compound 2), and $[H_3O]_4[Co_6(H_2O)_{22}\{Co_4(H_2O)_2P_4W_{30}O_{112}\}]\cdot 29H_2O$ (compound 3) (pz=pyrazine), were built from the linkage of $[Co_4(H_2O)_2(P_2W_{15}O_{56})_2]^{16-}$ (abbreviated as $\{Co_4P_4W_{30}\}$) polyanions and pz and/or cobalt(II) cations. Although compounds 1 and 2 consisted of the same components, their lamellar networks were quite different. The inorganic lamellar network in compound 3 was constructed by connecting $\{Co_4P_4W_{30}\}$ units with cobalt(II) cations. This work demonstrates that the coordination modes of $\{Co_4P_4W_{30}\}$ are very sensitive to synthesis conditions, while the ring-belt tetrametals are easily substituted by different transition metal cations under mild reaction conditions.

Key words: Cobalt; Crystal structure; Cyclic voltammetry; Hybrid; Polyoxometalate

1 Introduction

Polyoxometalates (POMs) are a unique class of nano-sized metal-oxygen clusters, which provide abundant oxygen donors to combine with transition metal cations for the construction of hybrid organic-inorganic coordination materials which exhibit distinctive topological framework structures and properties (Ma et al., 2019; Liu et al., 2020). Accompanying the development of synthesis strategy, the chemistry of POMs-based solid hybrid materials has been highly enriched by combining POMs, transition-metal cations, and organic moieties in organic-inorganic hybrid materials (Du et al., 2014; Ye and Wu, 2016; Li et al., 2021; Liao et al., 2021; Zhao et al., 2021).

The Weakley-type POMs, $[M_4(H_2O)_2(X_2W_{15}O_{56})_2]^{n-}$ (abbreviated as $\{M_4X_4W_{30}\}$, X=P^{V}, Si^{IV}, As^{V}, and Ge^{IV}, M=Mn^{II}, Co^{II}, Cu^{II}, and Zn^{II}), consist of tetrametal ring belts between two $\{X_2W_{15}O_{56}\}$ units, and have been used to modulate the properties of organic-inorganic hybrid materials for potential applications in different fields (Weakley and Finke, 1990; Gomez-Garcia et al., 1994; Kirby and Baker, 1995; Mbomekalle et al., 2003a, 2003b). The 30 $\{WO_6\}$ octahedra in the $\{M_4X_4W_{30}\}$ polyanion can be classified into three types that are grouped in two sets, including six cape, 12 middle, and 12 waist $\{WO_6\}$ octahedra, which are readily available to coordinate to metal cations for the construction of solid-state coordination materials (Fig. 1). However, incorporation of $\{M_4X_4W_{30}\}$ in a hybrid is not easily achieved with traditional synthesis methods, even using the most basic cluster $[\alpha\text{-}P_2W_{15}O_{56}]^{12-}$ as the starting material (Li et al., 2008, 2009). To understand the coordination ability of $\{M_4X_4W_{30}\}$, we report here on a "step-by-step aggregation" technology for rational fabrication of three $\{Co_4P_4W_{30}\}$-based hybrid materials: $[Co_8(H_2O)_{34}(pz)_2\{Co_4(H_2O)_2P_4W_{30}O_{112}\}]\cdot 16H_2O$ (compound 1), $[H_3O]_4[Co_6(H_2O)_{22}(pz)_2\{Co_4(H_2O)_2P_4W_{30}O_{112}\}]\cdot 21H_2O$ (compound 2), and $[H_3O]_4[Co_6(H_2O)_{22}\{Co_4(H_2O)_2P_4W_{30}O_{112}\}]\cdot 29H_2O$ (compound 3) (pz=pyrazine). The results reveal the important role of synthesis conditions in the formation of different $\{Co_4X_4W_{30}\}$-based hybrid coordination networks.

✉ Chuande WU, cdwu@zju.edu.cn
Chuande WU, https://orcid.org/0000-0001-8128-134X

Received May 9, 2023; Revision accepted July 12, 2023;
Crosschecked Jan. 17, 2024

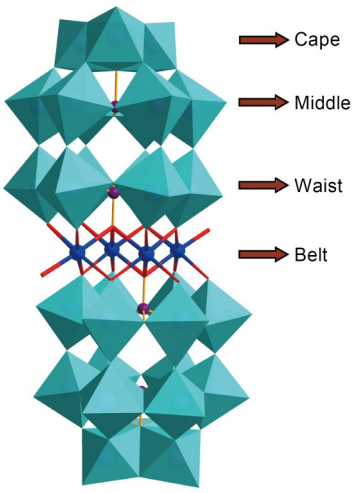

Fig. 1 Schematic of the Weakley-type polyanion $[M_4(H_2O)_2(X_2W_{15}O_{56})_2]^{n-}$ and the classification of the 30 $\{WO_6\}$ octahedra in the polyanion

2 Experimental

2.1 Materials and methods

All of the chemicals were obtained from commercial sources and were used without further purification, except for $Na_{16}[Co_4(H_2O)_2P_4W_{30}O_{112}]$ (abbreviated as $\{Co_4P_4W_{30}\}$) and $Na_{16}[Zn_4(H_2O)_2P_4W_{30}O_{112}]$ (abbreviated as $\{Zn_4P_4W_{30}\}$), which were synthesized as described by Finke et al. (1987). Infrared (IR) spectra were recorded from KBr pellets on an FTS-40 spectrophotometer (Bio-Rad, the USA) in the 4000–400 cm^{-1} region. We carried out thermogravimetric analyses (TGA) in N_2 atmosphere on a NETZSCH STA 409 PC/PG instrument (NETZSCH, Germany) at a heating rate of 10 °C/min. Powder X-ray diffraction (PXRD) data for Cu-Kα radiation were recorded on a RIGAKU D/MAX 2550/PC (λ=1.5406 Å) (Rigaku International Corporation, Japan). Inductively coupled plasma mass spectrometry (ICP-MS) analysis was performed on an XSeries II instrument (Thermo Fisher Scientific, the USA) by dissolving the crystalline samples in concentrated nitric acid. Cyclic voltammograms were obtained at room temperature with a CHI 630 electrochemical workstation (Shanghai Chenhua Instruments Limited, China). Platinum gauze was used as a counter electrode, and a saturated calomel electrode (SCE) was used as the reference electrode. The chemically bulk-modified carbon-paste electrodes (CPEs) were used as working electrodes.

2.2 Synthesis of compound 1

We dissolved $\{Co_4P_4W_{30}\}$ (0.1 g, 0.012 mmol) in 20 mL distilled water and adjusted the pH value to 5.3 with dilute HCl aqueous solution (pH=1). $Co(NO_3)_2\cdot 6H_2O$ (0.2 g, 0.69 mmol) was added to the mixture, which was heated and stirred at 65 °C for 12 h. We added pz (5 mg, 0.063 mmol) in 5 mL hot water dropwise into the solution. After heating the mixture at 65 °C for 8 d, red crystals were isolated by filtration, washed with water, and dried at room temperature. The yield was 35% (based on $\{Co_4P_4W_{30}\}$). Elemental analysis results were as follows. Analysis calculated for $C_8H_{112}Co_{12}N_4O_{184}P_4W_{30}$ (%) were 7.40 for Co and 57.72 for W. Found results (%) were 7.21 for Co and 56.33 for W. IR peaks (KBr pellet, cm^{-1}) were found at 1635 (m), 1425 (w), 1162 (w), 1086 (s), 1050 (m), 935 (s), 907 (s), 770 (s), and 727 (s) (Fig. S1 of the electronic supplementary materials (ESM)).

2.3 Synthesis of compound 2

The preparation procedure for compound 2 was similar to that for compound 1, except that we used $\{Zn_4P_4W_{30}\}$ (0.1 g, 0.012 mmol) instead of $\{Co_4P_4W_{30}\}$. The yield was 28% (based on $\{Zn_4P_4W_{30}\}$). Analysis calculated for $C_8H_{116}Co_9N_4O_{156}P_4W_{30}$ (%) were 5.94 for Co, and 61.73 for W. Found results (%) were 5.61 for Co, 0.35 for Zn, and 60.07 for W. IR peaks (KBr pellet, cm^{-1}) were found at 1624 (m), 1421 (w), 1166 (w), 1084 (s), 1051 (w), 1015 (w), 935 (s), 905 (w), and 716 (s) (Fig. S2).

2.4 Synthesis of compound 3

The preparation procedure for compound 3 was also similar to that for compound 1, except that we used 4, 4′-bipyridine (4, 4′-bpy) (0.5 mg, 0.003 mmol) instead of pz. The yield was 10% (based on $\{Co_4P_4W_{30}\}$). Analysis calculated for $H_{114}Co_{10}O_{167}P_4W_{30}$ (%) were 6.54 for Co and 61.18 for W. Found results (%) were 6.21 for Co and 60.73 for W. IR peaks (KBr pellet, cm^{-1}) were found at 1617 (m), 1489 (w), 1435 (m), 1409 (w), 1223 (w), 1086 (s), 1047 (w), 935.6 (s), 907 (s), and 769 (s) (Fig. S3).

2.5 Typical procedure for the preparation of CPEs based on compounds 1, 2, and 3

The solid material-modified CPE was fabricated as follows: 0.05 g graphite powder and 0.02 g solid

sample were mixed together with an agate mortar and pestle to achieve an even dried mixture. Next, 0.5 mL paraffin oil was added to the mixture and stirred with a glass rod. The resulting homogenized mixture was packed into a 3 mm inner diameter glass tube, and the surface was wiped with weighing paper. Electrical contact was established with a copper rod through the back of the electrode (Wang et al., 2010).

2.6 Single-crystal X-ray data collection and structural determination

We performed the determination of the unit cells and data collection for the crystals of each compound on an Oxford Xcalibur Gemini Ultra diffractometer with an Atlas detector. The data were collected using graphite-monochromatic Mo-Kα radiation (λ=0.71073 Å) at 293 K and the datasets were corrected by empirical absorption correction (Oxford Diffraction Ltd., 2010). The structures were solved by direct methods, and refined by full-matrix least-square methods with the SHELX-97 program package (Sheldrick, 1997). All non-solvent atoms were located successfully from Fourier maps. The solvent molecules in compounds 1–3 were highly disordered, and we used the SQUEEZE subroutine of the PLATON software suit to remove the scattering from the highly disordered water molecules (Spek, 2003). The resulting new files were used to further refine the crystal structures. The relatively high R_1 values for all three compounds should be ascribed to the relatively large system. The data-collection parameters, crystallographic data, and final agreement factors are collected in Table 1.

Table 1 Crystal data and structure refinements for compounds 1–3

Parameter	Description		
	Compound 1	Compound 2	Compound 3
Formula weight	9555.56	8934.80	9015.59
Crystal system	Triclinic	Triclinic	Monoclinic
a (Å)	14.2766 (8)	14.3599 (19)	28.113(6)
b (Å)	14.6461 (8)	14.619 (2)	14.5015 (14)
c (Å)	19.3539 (10)	20.987 (3)	22.634 (3)
α (°)	91.280 (4)	84.802 (10)	90.00
β (°)	90.004 (4)	88.526 (10)	115.88 (2)
γ (°)	105.867 (5)	73.651 (12)	90.00
Volume (Å^3)	3891.6 (4)	4210.4 (9)	8302 (2)
Space group	$P\bar{1}$	$P\bar{1}$	$C2/m$
Z	1	1	2
ρ (g/cm^3)	4.077	3.524	3.607
F(000)	4264	3963	8000
μ (mm^{-1})	23.486	21.400	21.808
Reflections collected	54475	20449	16664
Data/parameters	13714/928	11963/485	7639/415
R_{int}	0.0993	0.1384	0.0813
R_1 ($I>2\sigma(I)$)	0.1227	0.1389	0.1380
$wR(F^2)$ ($I>2\sigma(I)$)	0.2782	0.2884	0.3147
Goodness of fit on F^2	1.378	1.074	1.461

a, b, c, α, β, and γ: unit cell parameters; Z: the number of molecules in a unit cell; ρ: calculated density; F(000): the total number of electrons in a unit cell; μ: absorption coefficient; Data/parameters: number of independent reflections/number of structure refinement parameters; R_{int}: closeness of agreement in intensities for supposedly equivalent reflections; $R_1=\sum(|F_o|-|F_c|)/\sum|F_o|$, $wR=[\sum w(F_o^2-F_c^2)^2/\sum w(F_o^2)^2]^{0.5}$; I: intensity of the reflection; σ: standard uncertainty of a parameter; F_o: observed structure factor amplitude; F_c: calculated structure factor amplitude.

3 Results and discussion

The purity of the bulk samples of each compound was confirmed by comparing the PXRD diffraction peaks of simulated and experimental patterns (Figs. S4–S7). All of the typical vibrations were clearly visible in the IR spectra of the compounds. The IR spectra all exhibited strong bands around the peak of 1080 cm^{-1}, which we attributed to the asymmetric stretching vibration of the P-O bond (Finke et al., 1987). The characteristic bands of the terminal W-O vibrations of the Wells-Dawson units appeared at 935 cm^{-1} for compound 1, 934 cm^{-1} for compound 2, and 936 cm^{-1} for compound 3. The vibrations of the corner-sharing W-O-W moieties were found in the following bands: 906 cm^{-1} for compound 1, 906 cm^{-1} for compound 2, and 907 cm^{-1} for compound 3. The vibrations of the edge-sharing W-O-W moieties presented at 769 cm^{-1} for compound 1, 760 cm^{-1} for compound 2, and 765 cm^{-1} for compound 3 (Harmalker et al., 1983; Finke et al., 1987). We attribute the bands in the region of 1424–1162 cm^{-1} to the pz ligand in compounds 1 and 2 (Kong et al., 2006).

Heating a mixture of $\{Co_4P_4W_{30}\}$, $Co(NO_3)_2\cdot 6H_2O$, and pz in an acidified aqueous solution at 65 °C for 8 d afforded red crystals of compound 1. Single-crystal X-ray diffraction analysis revealed that compound 1 consisted of 2D lamellae based on $\{Co_4P_4W_{30}\}$, cobalt(II) cations, and pz ligands in P-1 symmetry (Fig. 2). In compound 1, $\{Co_4P_4W_{30}\}$ was built from two B-type $\{\alpha\text{-}P_2W_{15}O_{56}\}$ fragments and a sandwiched belt with

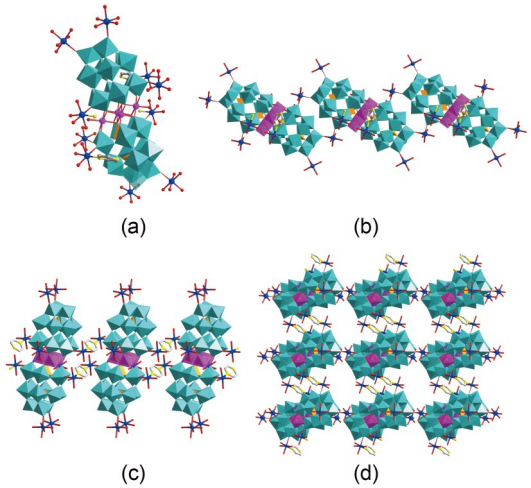

Fig. 2 (a) Ball-and-stick and polyhedral representations of the local structure for compound 1; (b) View of the 1D chain of $\{Co_4P_4W_{30}\}$ connected by the coordination connection between cobalt(II) cations and $\{WO_6\}$ octahedra in compound 1; (c) View of the 1D chain of $\{Co_4P_4W_{30}\}$ connected by the coordination connection between pz ligands and cobalt(II) cations; (d) Side view of the 2D lamellar coordination network in compound 1 (color codes: cyan: W; orange: P; purple and blue: Co; grey: C; yellow: N; red: O). References to color refer to the online version of this figure

four cobalt(II) cations, and all of the bond lengths and angles of $\{Co_4P_4W_{30}\}$ were within the normal ranges and consistent with those described in the literature (Finke et al., 1987).

The $\{Co_4P_4W_{30}\}$ unit acted as a decadentate ligand to coordinate to 10 cobalt(II) cations with 10 terminal oxygen atoms of 10 $\{WO_6\}$ octahedra (Fig. 2a). According to the coordination environment, there were three kinds of octahedrally coordinated cobalt(II) cations in compound 1, besides the cobalt(II) cations in the sandwiched ring belt of $\{Co_4P_4W_{30}\}$. The first cobalt(II) cation coordinates to one cape oxygen atom in $\{Co_4P_4W_{30}\}$, one waist oxygen atom in the neighboring $\{Co_4P_4W_{30}\}$, and four aqua ligands. Accordingly, two octahedrally coordinated cobalt(II) cations linked up two neighboring $\{Co_4P_4W_{30}\}$ units by coordinating to one cape and one waist $\{WO_6\}$ octahedron to extend into a linear network structure (Fig. 2b). The second cobalt(II) cation coordinated to one waist oxygen atom in $\{Co_4P_4W_{30}\}$, four water molecules, and one pz ligand, which further propagated into a polymeric chain linked by pz-bridging ligands (Fig. 2c). As a result, the $\{Co_4P_4W_{30}\}$ units were linked by cobalt(II) cations and pz bridging ligands to form an interesting thick lamellar network (Fig. 2d). The remaining two cobalt(II) cations terminated on the $\{Co_4P_4W_{30}\}$ unit, with five water ligands to fulfil the octahedral coordination environment. The TGA curve shows that a weight loss of 9.8% occurred between 30 and 245 °C, corresponding to the loss of water molecules (Fig. S8).

When we used $\{Zn_4P_4W_{30}\}$ instead of $\{Co_4P_4W_{30}\}$ under the same synthesis conditions used for compound 1, a lamellar coordination network of compound 2 was isolated as red crystals. Elemental analysis revealed that most of the zinc cations had been replaced by cobalt(II) cations. Since there was no Na^I cation in the crystal lattice, according to the elemental analysis results, we deduced that hydronium was maintaining the charge balance. Single-crystal X-ray structural analysis revealed that compound 2 was a lamellar network built from connecting cobalt(II) cations with $\{Co_4P_4W_{30}\}$ and pz units in P-1 symmetry (Fig. 3). It is worth noting that the coordination mode of a $\{Co_4P_4W_{30}\}$ unit in the lamellar network of compound 2 was different from that in compound 1. Each $\{Co_4P_4W_{30}\}$ acted as an octadentate ligand to coordinate to eight cobalt(II) cations by four middle and four waist oxygen atoms (Fig. 3a).

There are two kinds of cobalt(II) cations, classified according to their positions on $\{Co_4P_4W_{30}\}$. The first kind is penta-coordinated to two middle oxygen

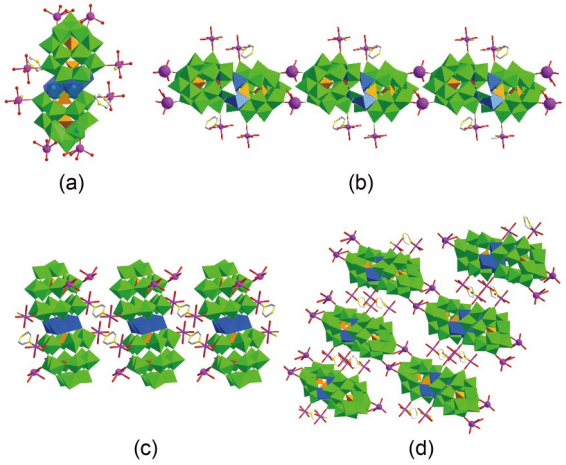

Fig. 3 (a) Ball-and-stick and polyhedral representations of the local structure for compound 2; (b) View of the 1D chain of $\{Co_4P_4W_{30}\}$ connected by cobalt(II) cations coordinating to the middle $\{WO_6\}$ octahedra in compound 2; (c) View of the 1D chain of $\{Co_4P_4W_{30}\}$ connected by pz bridging cobalt(II) cations in compound 2; (d) Side view of the 2D lamellar coordination network in compound 2 (color codes: green: W; orange: P; purple and blue: Co; grey: C; yellow: N; red: O). References to color refer to the online version of this figure

atoms of two neighboring $\{Co_4P_4W_{30}\}$ units and three water molecules, which links up the $\{Co_4P_4W_{30}\}$ units so that they can propagate into a linear network (Fig. 3b). Similar to the coordination mode in compound 1, the pz ligand was bidentately coordinated to the second kind of cobalt(II) cation in the waist of different $\{Co_4P_4W_{30}\}$ clusters, propagating into the second kind of chain (Fig. 3c). As a result, the $\{Co_4P_4W_{30}\}$ units were linked in two different ways to form a thick lamellar network (Fig. 2d). The TGA curve shows that a weight loss of 10.0% occurred between 30 and 185 °C, corresponding to the loss of water molecules (expected 9.9%) (Fig. S9).

When we used 4,4′-bipyridine (4,4′-bpy) instead of pz ligand under the same synthesis conditions used for compound 1, an interesting inorganic lamellar coordination network of compound 3 was isolated as red crystals. In the absence of 4,4′-bpy ligand under the same reaction conditions, only pink powder was isolated. This result indicates that 4,4′-bpy might play a crucial role in the formation of the crystals of compound 3. As there was no Na^{I} cation in the crystal lattice (according to elemental analysis results), the charge-balance cation should be hydronium. Single-crystal X-ray diffraction analysis revealed that compound 3 crystallized in the monoclinic *C*2/*m* space group, which consisted of 2D inorganic lamellae of $\{Co_4P_4W_{30}\}$ bridged by cobalt(II) cations (Fig. 4).

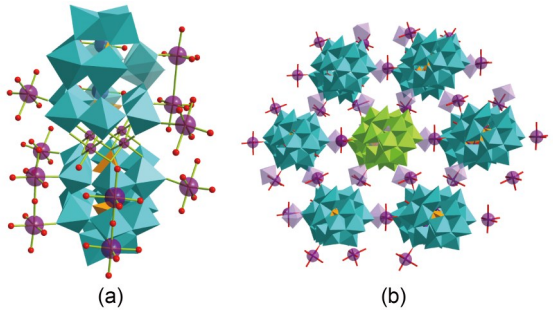

Fig. 4 (a) Ball-and-stick and polyhedral representations of the local structure for compound 3; (b) Top view of the 2D sheet in compound 3 (color codes: cyan and green: W; orange: P; purple: Co; red: O). References to color refer to the online version of this figure

There are four cobalt(II) cations located on the middle of $\{Co_4P_4W_{30}\}$, while the remaining eight cobalt(II) atoms are around the waist (Fig. 4a). Each $\{Co_4P_4W_{30}\}$ unit acted as a twelve-dentate ligand to coordinate to 12 cobalt(II) cations, besides the ring belt cobalt(II) ions in $\{Co_4P_4W_{30}\}$. The cobalt(II) cation octahedrally coordinated to one middle oxygen atom in $\{Co_4P_4W_{30}\}$ and one waist oxygen atom in the neighboring $\{Co_4P_4W_{30}\}$ unit on the apical sites, as well as four aqua ligands on the equatorial positions. As a result, each $\{Co_4P_4W_{30}\}$ cluster was bridged by 12 cobalt(II) cations to link up six neighboring $\{Co_4P_4W_{30}\}$ units, and further propagated into a lamellar network (Fig. 4b). The TGA curve shows that a weight loss of 11.1% occurred between 30 and 193 °C, corresponding to the loss of water molecules (expected 11.4%) (Fig. S10).

Because compounds 1–3 are insoluble in water and common organic solvents, these compounds have been used as modifiers to fabricate chemically modified CPE (Mbomekalle et al., 2003a, 2003b). We recorded the cyclic voltammetric behaviors for 1-, 2-, and 3-CPE in 1 mol/L H_2SO_4 aqueous solution at different scan rates. Compounds 1–3 exhibited three pairs of redox peaks in the potential range of 800 to −800 mV (Fig. 5). There were three reversible redox peaks: I-I′, II-II′, and III-III′, which should be ascribed to three consecutive two-electron processes of W centers (Ruhlmann et al., 2002, 2004, 2007; Bi et al., 2005; Mbomekalle et al., 2005; Schaming et al., 2009; Ammam et al., 2010). The half-wave potential $E_{1/2}$ was calculated by $(E_{pa}+E_{pc})/2$ (mV), where E_{pa} and E_{pc} are potential of oxidative peak and potential of reductive potential, respectively. They were −15.85 mV (I-I′), −220.1 mV (II-II′), and −397.1 mV (III-III′) for compound 1 (scan rate: 40 mV/s), 5.5 mV (I-I′), −221.5 mV (II-II′), and −391.5 mV (III-III′) for compound 2 (scan rate: 100 mV/s), and −13.1 mV (I-I′), −201.6 mV (II-II′), and −400 mV (III-III′) for compound 3 (scan rate: 200 mV/s). When the scan rate was gradually increased from 40 to 400 mV/s for these CPEs, the cathodic peak potentials were shifted in the negative direction and the corresponding anodic peak potentials were shifted in the positive direction. As shown in Fig. 5d, the cyclic peak currents are proportional to the scan rates (from 40 to 350 mV/s), suggesting that the redox process should be surface-controlled (Song et al., 1999; Ruhlmann et al., 2002, 2004, 2007; Schaming et al., 2009). It is worth noting that these CPEs were very stable after 20 manifold cyclic voltammetry cycles at a scan rate of 80 mV/s in the potential range of +0.8 to −0.6 V, revealing the high stability of these hybrid materials (Fig. S11).

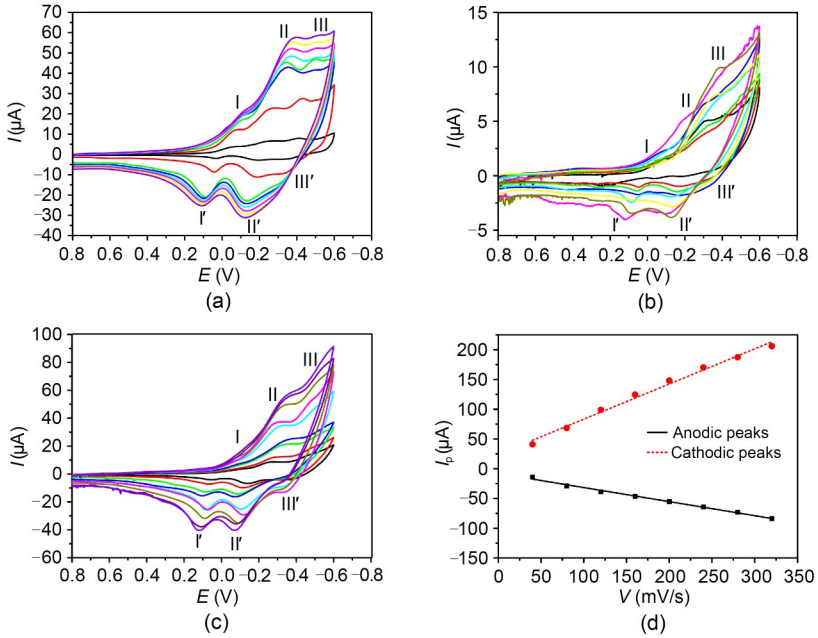

Fig. 5 Cyclic voltammetric behaviors (*I*-*E*) in 1 mol/L H_2SO_4 solution at different scan rates *V* (from inner to outer: 40, 80, 120, 160, 200, 240, 280, and 320 mV/s) for (a) 1-CPE, (b) 2-CPE, and (c) 3-CPE; (d) Dependences of cathodic peak (II) and anodic peak (II′) currents (I_p) for 1-CPE on scan rates from 40 to 350 mV/s

4 Conclusions

In summary, we successfully synthesized three $\{Co_4P_4W_{30}\}$ cluster-supported hybrid coordination materials under ambient reaction conditions. The slight differences in metal cations in the ring belt of $\{M_4P_4W_{30}\}$ are responsible for the formation of different hybrid materials with distinctive framework structures. Moreover, this work demonstrates for the first time that ring-belt tetrametals are easily replaced by environmental transition metal cations under ambient conditions. We believe that this work provides valuable information for the rational design and assembly of POM-based organic-inorganic hybrids for various potential applications.

Acknowledgments

This work is supported by the National Natural Science Foundation of China (Nos. 21525312 and 21872122).

Author contributions

Chuande WU designed the research. Jijie YE and Xuan XU processed the corresponding data, and wrote the first draft of the manuscript. Chuande WU revised and edited the final version.

Conflict of interest

Jijie YE, Xuan XU, and Chuande WU declare that they have no conflict of interest.

References

Ammam M, Mbomekalle IM, Keita B, et al., 2010. Electrochemical behavior and electrocatalytic properties towards hydrogen peroxide, dioxygen and nitrate of the polyanions $[(Ni^{II}OH_2)_2(Fe^{III})_2(X_2W_{15}O_{56})_2]^{14-}$ (X=PV or AsV): a comparative study. *Journal of Electroanalytical Chemistry*, 647(2):97-102. https://doi.org/10.1016/j.jelechem.2010.06.014

Bi LH, Shen Y, Jiang JG, et al., 2005. Electrochemical behavior and assembly of tetranuclear Dawson-derived sandwich compound $[Cd_4(H_2O)_2(As_2W_{15}O_{56})_2]^{16-}$ on 4-aminobenzoic acid modified glassy carbon electrode. *Analytica Chimica Acta*, 534(2):343-351. https://doi.org/10.1016/j.aca.2004.11.040

Du DY, Qin JS, Li SL, et al., 2014. Recent advances in porous polyoxometalate-based metal-organic framework materials. *Chemical Society Reviews*, 43(13):4615-4632. https://doi.org/10.1039/C3CS60404G

Finke RG, Droege MW, Domaille PJ, 1987. Trivacant heteropolytungstate derivatives. 3. Rational syntheses, characterization, two-dimensional 183W NMR, and properties of $P_2W_{18}M_4(H_2O)_2O_{68}^{10-}$ and $P_4W_{30}M_4(H_2O)_2O_{112}^{16-}$ (M=Co, Cu, Zn). *Inorganic Chemistry*, 26(23):3886-3896. https://doi.org/10.1021/ic00270a014

Gomez-Garcia CJ, Borras-Almenar JJ, Coronado E, et al., 1994. Single-crystal X-ray structure and magnetic properties of the polyoxotungstate complexes $Na_{16}[M_4(H_2O)_2(P_2W_{15}O_{56})_2]\cdot nH_2O$ (M=Mn^{II}, *n*=53; M=Ni^{II}, *n*=52): an

antiferromagnetic Mn^{II} tetramer and a ferromagnetic Ni^{II} tetramer. *Inorganic Chemistry*, 33(18):4016-4022. https://doi.org/10.1021/ic00096a028

Harmalker SP, Leparulo MA, Pope MT, 1983. Mixed-valence chemistry of adjacent vanadium centers in heteropolytungstate anions. 1. Synthesis and electronic structures of mono-, di-, and trisubstituted derivatives of α-$[P_2W_{18}O_{62}]^{6-}$. *Journal of the American Chemical Society*, 105(13):4286-4292. https://doi.org/10.1021/ja00351a028

Kirby JF, Baker LCW, 1995. Evaluations of a general NMR method, based on properties of heteropoly blues, for determining rates of electron transfer through various bridges. New mixed-mixed valence complexes. *Journal of the American Chemical Society*, 117(40):10010-10016. https://doi.org/10.1021/ja00145a011

Kong XJ, Ren YP, Zheng PQ, et al., 2006. Construction of polyoxometalates-based coordination polymers through direct incorporation between polyoxometalates and the voids in a 2D network. *Inorganic Chemistry*, 45(26):10702-10711. https://doi.org/10.1021/ic061664y

Li B, Zhao D, Zheng ST, et al., 2008. Hydrothermal synthesis and structural characterization of two organic-inorganic hybrids based on sandwich-type polyoxometalates. *Journal of Cluster Science*, 19(4):641-650. https://doi.org/10.1007/s10876-008-0218-1

Li B, Zhao D, Yang GY, 2009. Hydrothermal synthesis and structural characterization of three one-dimensional heteropolytungstates formed by mono-$copper^{II}$-substituted Dawson or Keggin cluster units. *Journal of Cluster Science*, 20(3):629-639. https://doi.org/10.1007/s10876-009-0264-3

Li Z, Zhang JH, Jing XT, et al., 2021. A polyoxometalate@covalent triazine framework as a robust electrocatalyst for selective benzyl alcohol oxidation coupled with hydrogen production. *Journal of Materials Chemistry A*, 9(10):6152-6159. https://doi.org/10.1039/D0TA09421H

Liao MY, Wang TM, Zuo T, et al., 2021. Design and solvothermal synthesis of polyoxometalate-based Cu(II)-pyrazolate photocatalytic compounds for solar-light-driven hydrogen evolution. *Inorganic Chemistry*, 60(17):13136-13149. https://doi.org/10.1021/acs.inorgchem.1c01540

Liu JX, Zhang XB, Li YL, et al., 2020. Polyoxometalate functionalized architectures. *Coordination Chemistry Reviews*, 414:213260. https://doi.org/10.1016/j.ccr.2020.213260

Ma PT, Hu F, Wang JP, et al., 2019. Carboxylate covalently modified polyoxometalates: from synthesis, structural diversity to applications. *Coordination Chemistry Reviews*, 378:281-309. https://doi.org/10.1016/j.ccr.2018.02.010

Mbomekalle IM, Keita B, Nadjo L, et al., 2003a. Lacunary Wells-Dawson sandwich complexes-synthesis, characterization, and stability studies of multi-iron species. *European Journal of Inorganic Chemistry*, 2003(21):3924-3928. https://doi.org/10.1002/ejic.200300345

Mbomekalle IM, Keita B, Nadjo L, et al., 2003b. Manganous heteropolytungstates. Synthesis and heteroatom effects in Wells-Dawson-derived sandwich complexes. *Dalton Transactions*, (13):2646-2650. https://doi.org/10.1039/B304255C

Mbomekalle IM, Cao R, Hardcastle KI, et al., 2005. Synthesis, structural characterization, and electrocatalytic studies of $\alpha\beta\beta\alpha$-$(Zn^{II}OH_2)_2(Fe^{III})_2(X_2W_{15}O_{56})_2^{14-}$ (X=P or As). *Comptes Rendus Chimie*, 8(6-7):1077-1086. https://doi.org/10.1016/j.crci.2004.10.010

Oxford Diffraction Ltd., 2010. CrysAlisPro, Version 1.171.33.56. Oxford Diffraction Ltd., UK. https://www.agilent.com/cs/library/usermanuals/public/CrysAlis_Pro_User_Manual.pdf

Ruhlmann L, Canny J, Contant R, et al., 2002. Di- and tricobalt Dawson sandwich complexes: synthesis, spectroscopic characterization, and electrochemical behavior of $Na_{18}[(NaOH_2)_2Co_2(P_2W_{15}O_{56})_2]$ and $Na_{17}[(NaOH_2)Co_3(H_2O)(P_2W_{15}O_{56})_2]$. *Inorganic Chemistry*, 41(15):3811-3819. https://doi.org/10.1021/ic020146u

Ruhlmann L, Canny J, Vaissermann J, et al., 2004. Mixed-metal sandwich complexes $[M^{II}_2(H_2O)_2Fe^{III}_2(P_2W15O_{56})_2]^{14-}$ (M^{II}= Co, Mn): synthesis and stability. The molecular structure of $[M^{II}_2(H_2O)_2Fe^{III}_2(P_2W_{15}O_{56})_2]^{14-}$. *Dalton Transactions*, (5):794-800. https://doi.org/10.1039/B315088G

Ruhlmann L, Costa-Coquelard C, Canny J, et al., 2007. Mixed-metal Dawson sandwich complexes: synthesis, spectroscopic characterization and electrochemical behaviour of $Na_{16}[M^{II}Co_3(H_2O)_2(P_2W_{15}O_{56})_2]$ (M=Mn, Co, Ni, Zn and Cd). *European Journal of Inorganic Chemistry*, 2007(11):1493-1500. https://doi.org/10.1002/ejic.200600942

Schaming D, Canny J, Boubekeur K, et al., 2009. An unprecedented trinuclear Dawson sandwich complex with internal lacuna: synthesis and ^{31}P NMR spectroscopic analysis of the symmetrical $[NaNi_3(H_2O)_2(P_2W_{15}O_{56})_2]^{17-}$ and $[CoNi_3(H_2O)_2(P_2W_{15}O_{56})_2]^{16-}$ anions. *European Journal of Inorganic Chemistry*, 2009(33):5004-5009. https://doi.org/10.1002/ejic.200900738

Sheldrick GM, 1997. SHELXL-97: Program for the Refinement of Crystal Structures. University of Göttingen, Göttingen, Germany.

Song WB, Wang XH, Liu Y, et al., 1999. Electrochemical and electrocatalytic properties of tetra-iron substituted sandwich-type pentadecatungstodiphosphate heteropolyanions. *Journal of Electroanalytical Chemistry*, 476(1):85-89. https://doi.org/10.1016/S0022-0728(99)00363-0

Spek AL, 2003. Single-crystal structure validation with the program PLATON. *Journal of Applied Crystallography*, 36(1):7-13. https://doi.org/10.1107/S0021889802022112

Wang XL, Hu HL, Tian AX, 2010. Influence of transition metal coordination nature on the assembly of multinuclear subunits in polyoxometalates-based compounds. *Crystal Growth & Design*, 10(11):4786-4794. https://doi.org/10.1021/cg1006742

Weakley TJR, Finke RG, 1990. Single-crystal X-ray structures of the polyoxotungstate salts $K_{8.3}Na_{1.7}[Cu_4(H_2O)_2(PW_9O_{34})_2]\cdot 24H_2O$ and $Na_{14}Cu[Cu_4(H_2O)_2(P_2Wl_5O_{56})_2]\cdot 53H_2O$. *Inorganic Chemistry*, 29(6):1235-1241. https://doi.org/10.1021/ic00331a025

Ye JJ, Wu CD, 2016. Immobilization of polyoxometalates in crystalline solids for highly efficient heterogeneous catalysis. *Dalton Transactions*, 45(25):10101-10112. https://doi.org/10.1039/C6DT01378C

Zhao HY, Li YZ, Zhao JW, et al., 2021. State-of-the-art advances in the structural diversities and catalytic applications of polyoxoniobate-based materials. *Coordination Chemistry Reviews*, 443:213966. https://doi.org/10.1016/j.ccr.2021.213966

Electronic supplementary materials

Figs. S1–S11